TITLE PAGE

Experimental colitis drives enteric alpha-synuclein accumulation and Parkinson-like brain pathology

Stefan Grathwohl[1], Emmanuel Quansah[2], Nazia Maroof[1], Jennifer A. Steiner[2], Liz Spycher[1], Fethallah Benmansour[3], Gonzalo Duran-Pacheco[4], Juliane Siebourg-Polster[4], Krisztina Oroszlan-Szovik[1], Helga Remy[1], Markus Haenggi[1], Marc Stawiski[1], Matthias Sehlhausen[4], Pierre Maliver[4], Andreas Wolfert[5], Thomas Emrich[5], Zachary Madaj[2], Martha L. Escobar Galvis[2], Christoph Mueller[6], Annika Herrmann[4], Patrik Brundin[2], and Markus Britschgi[1]

[1] Roche Pharma Research and Early Development, Neuroscience Discovery, Roche Innovation Center Basel, F. Hoffmann-La Roche Ltd, Grenzacherstrasse 124, Basel, Switzerland

[2] Center for Neurodegenerative Science, Van Andel Research Institute, 333 Bostwick Ave. NE, Grand Rapids, MI, USA

[3] Roche Pharma Research and Early Development, pREDi, Roche Innovation Center Basel, F. Hoffmann-La Roche Ltd, Grenzacherstrasse 124, Basel, Switzerland

[4] Roche Pharma Research and Early Development, Pharmaceutical Sciences, Roche Innovation Center Basel, F. Hoffmann-La Roche Ltd, Grenzacherstrasse 124, Basel, Switzerland

[5] Roche Pharma Research and Early Development, Pharmaceutical Sciences, Roche Innovation Center Munich, Roche Diagnostics GmbH, Nonnenwald 2, 82377 Penzberg, Germany

[6] Institute of Pathology, University of Bern, Murtenstrasse 31, Bern, Switzerland

Corresponding authors:

Markus Britschgi, Roche Pharma Research and Early Development, Neuroscience Discovery, Roche Innovation Center Basel, F. Hoffmann-La Roche Ltd, Grenzacherstrasse 124, Basel, Switzerland

Tel: +41 61 6879116

Email: markus.britschgi@roche.com

Patrik Brundin, Van Andel Research Institute, 333 Bostwick Ave. NE, Grand Rapids, MI 49503, USA.

Tel: +1 616.234.5312

Email: patrik.brundin@vai.org

Abstract

Intraneuronal accumulation of α-synuclein (αSyn) is key in the pathogenesis of Parkinson's disease (PD). Published studies suggest that this process begins in the enteric nervous system (ENS) and propagates into the brain decades before clinical diagnosis of PD. The triggers and mechanisms underlying the accumulation of αSyn remain unknown but evidence is growing, that immune pathways and in particular colitis may play a critical role. Here we demonstrate that patients with inflammatory bowel disease (IBD) exhibit αSyn accumulation in their colon. We then confirmed in an experimental model of IBD that intestinal inflammation can trigger αSyn accumulation in the ENS of wildtype and αSyn transgenic mice. We discovered that the type and degree of inflammation modulates the extent of αSyn accumulation in the colon and that macrophage-related signaling limits this process. Remarkably, experimental colitis at three months of age exacerbated the accumulation of aggregated phospho-Serine 129 αSyn in the midbrain, including the substantia nigra, in 21-month but not 9-month-old αSyn transgenic mice. This was accompanied by loss of nigral tyrosine hydroxylase-immunoreactive neurons, another neuropathological hallmark of PD. Together, our data suggest a critical role for intestinal inflammation in the initiation and progression of PD.

Introduction

Parkinson's disease (PD) is a progressively debilitating neurodegenerative disease affecting 1% of the population above 60 years (1). Typical symptoms are motor impairments including muscle rigidity, tremor, and bradykinesia. Neuropathologically, PD is hallmarked by dopaminergic cell loss in the substantia nigra (SN), a resultant loss of striatal dopaminergic signaling (2, 3), and the presence of intraneuronal inclusions called Lewy bodies and neurites (4, 5). Lewy pathology is enriched in α-synuclein (αSyn), a presynaptic protein that tends to misfold, aggregate, and become phosphorylated under pathological conditions (2, 3). Alpha-synuclein is also genetically linked to rare familial forms of PD and certain SNPs close to the αSyn gene (*SNCA*) locus are associated with an increased risk for developing PD (6). These findings in humans make αSyn a focal point of biomarker and drug development programs for PD.

Several years before the first appearance of motor features, many patients exhibit a variety of non-motor symptoms including constipation, sleep disorder, depression, and hyposmia (7–9). Co-occurrence of some of these non-motor symptoms increases the risk of progressing to PD even in otherwise healthy individuals in population-based and cohort studies (10–13). Constipation may be a particularly important non-motor feature of preclinical PD, with 28-61% of patients often exhibiting gastrointestinal dysfunction years before progressing to motor symptoms (9, 12, 14). This suggests an early connection between the status of the intestinal environment and the progression to PD (15). In line with this connection and due to the discovery of αSyn immunoreactive inclusions in neurons of the submucosal plexus in people with PD, Braak and colleagues have suggested an early involvement of the enteric nervous system (ENS) in the pathogenesis of PD (4, 5, 16, 17). It is currently unclear, whether occurrence of αSyn aggregates in the peripheral nervous system is specific for PD since individuals with dementia with Lewy bodies and normal people can also show such inclusions in various tissues (18–21). Yet based on their findings, Braak and colleagues hypothesized that αSyn immunoreactive inclusions first appear in the ENS and then progress over time to the brainstem regions, including the dorsal motor nucleus of the vagus nerve and midbrain areas (4, 5, 16, 17). Several studies in preclinical models have recently demonstrated a potential propagation of αSyn

77 pathology in the gut and the brain (22–26). Intriguingly, a clinical study reported that vagotomy in a
78 Danish population decreases the risk of PD (27). Determining the critical factors for αSyn pathology
79 in the ENS could provide insights into disease etiology, enabling the development of novel treatment
80 paradigms to slow disease progression. A key factor that could trigger ENS αSyn accumulation and
81 pathology spread is inflammation.

82 Interestingly, a recent finding in children with gastrointestinal inflammation suggests an immune
83 regulatory function of αSyn (28). Immune pathways are indeed activated in the brain and colon of PD
84 cases (29, 30). Also, several genes associated with an increased risk of developing PD have an
85 immune system-related function (31), and a recent genome-wide association study identified common
86 genetic pathways linking PD and autoimmune disorders (32). Most prominently, LRRK2, a major
87 genetic risk factor for PD also confers increased risk for developing inflammatory bowel disease
88 (IBD) (33) and is known to modulate the function of monocytes, macrophages and other immune cells
89 (34, 35). Intriguingly, IBD is now confirmed to be associated with an increased risk for developing
90 PD and specifically blocking the TNF pathway reduces this risk (36–38).

91 Here we tested the hypothesis that intestinal inflammation (e.g. colitis) triggers αSyn aggregation in
92 the ENS and the subsequent development of αSyn pathology in the brain. We discovered that patients
93 with IBD exhibited increased αSyn accumulation in the submucosal region of the colon. Experimental
94 colitis in wild type and αSyn transgenic mice demonstrated that the type and degree of inflammation
95 modulates the extent of αSyn accumulation in the colon and that macrophage-related signaling limits
96 this process. Remarkably, experimental colitis at 3 months of age exacerbated the accumulation of
97 aggregated αSyn in midbrain, including the substantia nigra, in 21-month but not 9-month-old αSyn
98 transgenic mice. This was accompanied by loss of nigral tyrosine hydroxylase-immunoreactive
99 neurons. Together, our data suggest a critical role for intestinal inflammation in the initiation and
100 progression of PD.

Results

IBD patients show αSyn accumulation in the ENS and local macrophages

Recent epidemiological data links inflammatory bowel disease (IBD) to an increased risk of developing PD (36–38). In order to explore if IBD is associated with enteric αSyn accumulation we performed immunohistochemistry for αSyn in cryo-sections from colonic biopsies of patients with ulcerative colitis (UC, n = 11, mean age 31 years), Crohn's disease (CD, n = 11; mean age 35 years), and from normal controls (NC, n = 8; mean age 51 years). We observed in eight UC cases various degrees of αSyn accumulation, mostly in neuritic structures (**Figure 1A-C**). Interestingly, the eight UC cases, and four patients with CD also showed marked intracellular αSyn staining in many infiltrating monocytic cells. In contrast, only one NC subject showed a few immunoreactive cells. This finding in human tissue suggests a potential role of local inflammation in the development of enteric αSyn accumulation.

Experimental IBD exacerbates αSyn load in submucosal plexus of αSyn transgenic and wildtype mice

During the process of further characterizing a (Thy1)-h[A30P]αSyn transgenic mouse line (39) we detected human αSyn accumulation in all innervated organs that were analyzed (**Supplemental Figure 1**). This included the myenteric and submucosal plexuses of the ENS, where it co-localized with peripherin, a specific marker for peripheral nerves (**Figure 2A).** We observed an age-dependent increase of baseline αSyn inclusion in both plexuses between the age of three and twelve months (**Figure 2B**). Since this transgenic model has the capacity to increase the αSyn load in the ENS over time we wanted to test the hypothesis whether IBD- related inflammation in the colon may trigger or exacerbate local αSyn accumulation. Administration of dextran sodium sulfate (DSS) in the drinking water in acute or chronic paradigms is a well-established mouse model of IBD colitis, resulting in infiltration of leukocytes into the submucosa with various degrees of destruction of the colonic tissue and the mucosa (40). We administered DSS at different concentrations and durations to (Thy1)-h[A30P]αSyn transgenic mice (**Figure 2C**), resulting in leukocyte infiltration in a dose-dependent manner (**Figure 2D and 3A**). Intriguingly, in the acute paradigm, 2.5% but not 1% DSS triggered

129 intracellular accumulation of αSyn in the submucosal plexus **(Figure 3A and 3B)**. In the chronic DSS
130 paradigm, a dose-dependent increase of αSyn load in the submucosal plexus was observed **(Figure**
131 **3A and 3B)**. To confirm that this finding was not related to a transgene effect, an acute and a chronic
132 (consistent dose) DSS paradigm was respectively applied also in wildtype mice. In both paradigms,
133 we observed aggregation of endogenous murine αSyn in the submucosal plexus **(Figure 3C and 3D)**.
134 A separate experiment also confirmed that the observed effects of DSS could not be attributed to
135 increased gene expression of murine or the transgenic human αSyn **(Supplemental Figure 2)**.
136 Together, these results confirmed the validity of this experimental IBD paradigm to test the effect of
137 inflammation on αSyn accumulation in the ENS.
138
139 ***Colitis induced by peroral DSS but not by peritoneal administration of LPS aggravates αSyn***
140 ***accumulation in colonic submucosal plexus of αSyn transgenic mice***
141 In order to explore effects of different approaches to induce inflammation in or nearby the gut in
142 (Thy1)-h[A30P]αSyn transgenic mice, we compared the outcome of an acute 5% DSS in drinking
143 water with acute intraperitoneal LPS administration (**Figure 2C**). At d7, both agents had induced
144 variable degrees of leukocyte infiltration in the submucosa of the colon with a marked destruction of
145 the mucosa induced by only DSS (**Figure 2D and 4A**). Here, the DSS-exposed mice presented with
146 increased mean accumulation of αSyn in the ganglia of the submucosal plexus, higher than in the
147 2.5% DSS-exposed mice in the previous experiment (**Figure 4B-F**). In contrast, no change in αSyn
148 load was detected in the myenteric plexus, consistent with lack of leukocyte infiltration in this
149 anatomical region of the colon. Interestingly, LPS-induced inflammation did not increase αSyn
150 accumulation in the colonic nervous plexuses (**Figure 4C and E**). The two inflammatory insults
151 resulted, however, in a differential expression of cytokines, and consistent with leukocyte recruitment,
152 CCL2 was elevated in both (**Figure 4G and H**). Interestingly, in the LPS paradigm, mRNA for IL-10
153 was markedly elevated, whereas DSS strongly increased IL-6 and to some extent also IL-1β but not
154 IL-10. Together these results indicate that certain types of local inflammation can increase the
155 intracellular accumulation of aggregated αSyn in the periphery (i.e. in the colon).
156

157 ***Lack of Cx3cr1 signaling during DSS colitis aggravates αSyn load in the submucosal plexus of***
158 ***αSyn transgenic mice***
159 In both the IBD patients as well as the (Thy1)-h[A30P]αSyn transgenic mice that experienced acute
160 DSS colitis, we observed αSyn positive infiltrating cells (**Figure 5C and Figure 5D-F**). In the mice
161 these infiltrating cells were positive for the macrophage marker Iba-1 (**Figure 5G**). In order to explore
162 further the role of monocytes/macrophages in the accumulation of αSyn in our DSS model, we added
163 an experimental arm with (Thy1)-h[A30P]αSyn transgenic mice crossed with mice that have a
164 deletion of Cx3cr1 induced by an insertion of GFP (Cx3cr1-GFP knock-in mice). The CX3CR1-
165 CX3CL1 axis plays an important role in maintaining the function of the lamina propria macrophage
166 population of the gastrointestinal wall and lack of this signaling pathway in experimental colitis
167 models may either aggravate or ameliorate the induced pathology (41–43). In our experiment
168 exposure to DSS resulted in leukocyte infiltration in the Cx3cr1-deficient αSyn transgenic mice at a
169 minimally higher mean percent leukocyte area covered than for the Cx3cr1-competent group (**Figure**
170 **3A**). We observed, however, a significantly higher mean level of αSyn accumulated in the
171 submucosal plexus in αSyn transgenic mice lacking Cx3cr1 compared to αSyn transgenic mice
172 expressing Cx3cr1 ($p = 0.001$, two-way ANOVA with Tukey HSD post-hoc analysis; **Figure 3F**).
173 Consistent with the Cx3cr1-sufficient αSyn transgenic mice, no overt increased accumulation of αSyn
174 was observed in the myenteric plexus **(Figure 3D)**. These results indicate a potential link between
175 monocyte/macrophage signaling and αSyn accumulation in ENS in this experimental IBD model.
176
177 ***Systemic IL-10 ameliorates DSS-induced colitis and associated enteric αSyn accumulation in αSyn***
178 ***transgenic mice***
179 Interleukin-10 is an important regulator of monocytes/macrophages, and genetic ablation of IL-10
180 signaling or blocking IL-10 with specific antibodies was shown to enhance DSS colitis (44, 45).
181 Interestingly, we observed above that LPS-induced colonic leukocyte infiltration did not result in
182 increased accumulation of αSyn in the ENS of the colon and that the main difference in cytokine
183 expression between the DSS and LPS paradigms was increased IL-10 expression in the LPS group
184 (**Figure 3G and H**). To mimic the effect of higher levels of IL-10 in an acute model of DSS colitis,

185 we administered intravenously murine IL-10 (mIL10), which was recombinantly engineered onto two
186 different murine IgG variants to extend the half-life of mIL-10 in circulation (mIgG1(v1)-mIL10 and
187 mIgG1(v2)-mIL10, respectively). As shown previously, DSS induced a marked increase in leukocyte
188 infiltration and αSyn accumulation, which was similar in the untreated and control IgG treated group
189 (**Figure 4**). Both mIgG1(v1)-mIL10 and mIgG1(v2)-mIL10 significantly reduced leukocyte
190 infiltration despite administration of DSS ($p<0.0001$, one-way ANOVA with Tukey HSD post-hoc
191 analysis; **Figure 4A**). Both mIgG1-mIL10 variants also had reduced mean levels of human αSyn in
192 the submucosal plexus whereas mIgG1(v2)-mIL10 reached significance ($p=0.02$, one-way ANOVA
193 with Tukey HSD post-hoc analysis; **Figure 4B**). Interestingly, the significantly reduced αSyn
194 accumulation was associated with detectable serum exposure of mIgG1(v2)-mIL10 whereas
195 mIgG1(v1)-mIL10 was no longer detectable at the end of the in vivo phase, after 7d (**Figure 4**). These
196 results underline further an important role for the IL-10 pathway in keeping αSyn accumulation at a
197 reduced level throughout the course of experimental IBD. Together, the genetic and pharmacological
198 modulation of DSS colitis corroborates a relevant role for monocyte/macrophage pathways in the
199 development of αSyn accumulations in the ENS of the colon.
200
201 ***Experimental colitis-induced enteric αSyn accumulation persists for months and exacerbates brain***
202 ***pathology and dopaminergic cell loss in αSyn transgenic mice***
203 The previously highlighted hypothesis by Braak and colleagues associates αSyn brain pathology with
204 previous development of αSyn pathology in the ENS (5, 46). However, it is currently unknown
205 whether previous inflammatory conditions propel this ENS αSyn accumulation that may further
206 worsen αSyn aggregation in the brain. To test this, we first explored αSyn accumulation in the
207 submucosal plexus of (Thy1)-h[A30P]αSyn transgenic mice that had experienced DSS colitis
208 previously but had fully recovered two months later. As expected, leukocyte infiltration in the
209 submucosal plexus had returned to normal levels following the two-month recovery period
210 (**Supplemental Figure 3A**). Remarkably however, αSyn accumulation in the ganglia of the
211 submucosal plexus was still almost two-fold higher when compared to αSyn transgenic mice that were

212 not exposed to DSS, and this was exacerbated in αSyn transgenic mice deficient for Cx3cr1
213 (**Supplemental Figure 3B**).
214
215 To assess development of brain αSyn pathology, we exposed 3-month old hemizygous (Thy1)-
216 h[A30P]αSyn transgenic mice to DSS or normal drinking water (chronic increasing dose paradigm)
217 and then returned all to normal drinking water (**Figure 1C**). After aging up to 9 or 21 months of age
218 (i.e. mice aged for an additional 6 or 18 months after the chronic DSS paradigm), various brain
219 regions were analyzed for pathologically accumulated αSyn (proteinase K resistant, pSer129-αSyn
220 immunoreactive inclusions). Twenty-one month old mice that only received water during their
221 lifetime showed low levels of pathological αSyn inclusions in the brain (**Figure 6 and Supplemental**
222 **Figure 4**), which is consistent with previous observations in the brain of these hemizygous (Thy1)-
223 h[A30P]αSyn transgenic mice (47). In marked contrast, the majority of 21-month-old and previously
224 DSS-exposed αSyn transgenic mice presented with higher degrees of pathological αSyn in the same
225 brain areas where mice on water displayed much lower pSer129-positive immunoreactivity.
226 Intriguingly, mice that were aged to 9 months presented with extremely low levels of pathological
227 αSyn inclusions in the brain (**Figure 6 and Supplemental Figure 4**). For the mice that aged up to 21
228 months, the accumulated αSyn pathology recorded in the SN was accompanied by a significant loss of
229 tyrosine hydroxylase (TH) and Nissl positive cells ($p \leq 0.05$, Student's T-test; **Figure 7**). Together,
230 DSS colitis at a young age caused an age-dependent exacerbation of αSyn inclusion pathology in the
231 brain and a loss of nigral dopaminergic cells, similar to the human neuropathological hallmarks of PD.

232 **Discussion**

233 Currently, there is no therapy for PD available to slow or stop its progression and an obstacle in the
234 quest to develop one is that we do not understand the triggers of PD (48). Intraneuronal accumulation
235 of aggregated αSyn (i.e. Lewy bodies and neurites) is a key neuropathological hallmark, thus the
236 distribution of Lewy pathology in postmortem brain tissues has been used for disease staging in PD
237 (2, 4, 46). Abnormal accumulation of αSyn has also been observed in the peripheral nervous system in
238 PD and in some individuals at risk of developing the disease (49, 50). Similar to this finding in
239 people, αSyn immunoreactive inclusions have also been detected in the ENS of a transgenic mouse
240 model prior to changes in the CNS (51). It is also suggested, based on preclinical models and
241 postmortem pathology in various organs including the brain, that αSyn pathology propagates in a
242 temporospatial and prion-like manner (2, 4, 5, 52, 53). However, the initial factors triggering αSyn
243 aggregation are yet to be established (48). Moreover, the involvement of peripheral stimuli in the
244 aggregation and pathogenic spread of αSyn is only beginning to unravel.

245 In this study, we provide evidence that patients with IBD have increased αSyn accumulation in their
246 ENS (**Figure 1**) and that a IBD-like inflammation (DSS colitis) triggers αSyn accumulation in the
247 ENS of wildtype mice and in a transgenic mouse model of PD (**Figure 3**). Interestingly, in IBD
248 patients and in the mouse model of IBD, macrophages filled with αSyn could be observed in the
249 inflamed area (**Figure 5**). Aggravation of enteric αSyn accumulation in αSyn transgenic mice lacking
250 Cx3cr1 signaling and amelioration of inflammation and enteric αSyn load by systemic IL-10 suggest a
251 modulatory role of monocytes/macrophages in this process (**Figure 4 and 6**). Remarkably, we further
252 observed that the aggravation of αSyn accumulation in the ENS persisted even after two months of
253 recovery from DSS colitis, indicating that the observed effect is not a transient phenomenon
254 (**Supplemental Figure 3**). Most importantly, 18 months but not 6 months post DSS colitis, αSyn
255 trasngenic mice had developed a Parkinson-like pathology in their brain (**Figure 7 and 8 and**
256 **Supplemental Figure 4**). This included elevated proteinase K resistant pSer129-αSyn pathology in
257 the midbrain in the midbrain, including the substantia nigra, and other brain regions and an average
258 decrease of 30-50% of TH- and Nissl positive cells in the SN. Together, this colitis mouse model

259 recapitulated the proposed accumulation of αSyn in the ENS long before clinical diagnosis of PD in
260 humans and the subsequent age-related development of αSyn pathology in the brain, together with the
261 loss of nigral dopaminergic neurons.

262 We established that a mechanism by which peripheral inflammation promote αSyn accumulation in
263 the colon potentially involves monocytes and macrophages. Interestingly, both peroral DSS and
264 peritoneal LPS administration provoked strong local immune reactions resulting in leukocyte
265 infiltration into the submucosa of the colon. This inflamed region is anatomically right next to the
266 submucosal plexus and is separated by a muscular layer from the myenteric plexus (**Figure 2**). This
267 might explain why the effect of αSyn accumulation was only observed in the nerves of the
268 submucosal plexus but not in the ganglia of the myenteric plexus in our (Thy1)-h[A30P]αSyn
269 transgenic mouse model of colitis. The mechanism underlying how intraperitoneally administered
270 LPS leads to submucosal leukocyte infiltration probably involves the monocyte attractant chemokine
271 CCL2 (**Figure 4**), but the specifics remain unclear. CCL2 was also upregulated in the colon of our
272 DSS model. However, in contrast to peritoneal LPS, where infiltration of macrophages followed a
273 patchy pattern, DSS-related macrophage infiltration was distributed across the whole submucosa.
274 Also, the primary mechanism of peroral administered DSS is to destruct the mucosa of the colon,
275 similar to some forms of ulcerative colitis, resulting in the transient disintegration of the intestinal
276 epithelial barrier. The subsequent immune response to the infiltration of commensal bacteria evoked
277 also in our (Thy1)-h[A30P]αSyn transgenic mouse model the expression of cytokines such as IL-1β
278 and IL-6. This upregulation was absent in the LPS paradigm that had an intact mucosa. By acting on
279 tight junctions, IL-1β and IL-6 can increase intestinal barrier permeability (gut leakiness), facilitating
280 the recruitment of additional immune cells to the site of the inflammatory signal eventually
281 culminating in widespread immune activation (54, 55). Consistent with the breach of barrier
282 permeability in our mouse model, some PD patients express increased colonic cytokines such as IL-
283 1β, IL-6 and TNF, occurring together with increased intestinal permeability (29, 56). In this context, it
284 is striking that IBD patients on anti-TNF therapy have a reduced risk of developing PD (37). Here we
285 demonstrate that patients with IBD also present with αSyn accumulations in the ENS as well as in

286 infiltrating leukocytes nearby. In this regard, it is interesting to note that mucosal macrophages with
287 intralysosomal αSyn content were previously described in the intact human appendix (57). These
288 macrophages were in close proximity to the axonal varicosities of the vermiform appendix which
289 showed an enriched staining for αSyn in the mucosal plexus. Indeed, we recently demonstrated that
290 the vermiform appendix contains aggregated and truncated αSyn that has the propensity to aggregate
291 recombinant αSyn *in vitro* (18). Also, monomeric and oligomeric αSyn reportedly act as
292 chemoattractants for neutrophils and monocytes, enhancing the maturation of dendritic cells in the
293 ENS (28, 58). With such a role in intestinal immunity therefore, it is possible that the strong tissue
294 destruction induced by DSS in the present study released αSyn, which perhaps served as a
295 chemoattractant for monocytes. It is likely that increased abundance of extracellular αSyn and altered
296 intestinal permeability, along with the DSS-evoked inflammatory response may have provided an
297 enabling milieu allowing further αSyn accumulation in the ENS of the colon (59). However, the
298 pathways leading to αSyn accumulation in macrophages remain to be elucidated. Mechanistically, it
299 has been shown that excess endogenous αSyn compromises phagocytic activity in human iPSC-
300 derived macrophages (60). Macrophages and other immune cells are also regulated by LRRK2, an
301 established risk gene for PD and IBD. It will be interesting to explore in our colitis paradigm the
302 effect of LRRK2 (e.g. its effect on autophagy in macrophages (34, 35, 61)) and other pathways in
303 macrophages on αSyn accumulation.

304 Most profoundly, besides the accumulation of αSyn in the submucosal plexus, we found that a single
305 chronic DSS paradigm at young age exacerbated αSyn pathology in the CNS of (Thy1)-h[A30P]αSyn
306 transgenic mice later in life (**Figure 7**). But how does this severe αSyn inclusion pathology develop in
307 the brain of these mice? One hypothesis is that the brain αSyn pathology observed in this study could
308 be due to direct effects of peripheral immune activation on the brain and brain vasculature.
309 Hypothetically, colitis induced by DSS or LPS could compromise both active and passive components
310 of the blood-brain barrier, which may render the CNS vulnerable to immune cells from the periphery
311 (62, 63). Alternatively, certain peripheral triggers can directly affect microglial activity in the brain.
312 For instance, short-chain fatty acids derived from gut microbiota appear to regulate function and

313 maturation of microglia in the mouse CNS (64) and inflammatory mediators from gut microbiota
314 could be carried in the bloodstream and induce pathological and behavioral changes in an αSyn
315 transgenic mouse model (65). Moreover, rats and nematodes develop αSyn inclusions after exposure
316 to the bacterial amyloid protein curli, a protein which stimulates microgliosis, astrogliosis, and
317 secretion of IL-6 and TNF (66). Intriguingly, a recent study reported that peripherally applied
318 inflammatory stimuli induce acute immune training (that exacerbates β-amyloid pathology) and
319 immune tolerance in the brain that reprograms microglia, an effect which can persist for at least six
320 months (67).

321 Another hypothesis is that the brain αSyn pathology observed may have accumulated following the
322 transfer of pathogenic αSyn seeds from the gut via the vagal nerve. It is already established in rodents
323 and non-human primates that αSyn pathology in the CNS can propagate from cell to cell, perhaps in a
324 prion-like fashion (52, 53, 68, 69) and that certain pathogenic forms of αSyn may serve as templates
325 in recipient cells, seeding and inducing further aggregation of endogenous αSyn in these cells (68, 70–
326 72). Interestingly, several studies in preclinical *in vivo* models have demonstrated that pathogenic
327 αSyn seeds can be transferred from the peripheral nervous system to the CNS. Indeed, aggregated
328 recombinant αSyn injected intraperitoneally, intramuscularly or into the gastric wall of certain mouse
329 models of PD results in αSyn inclusions in the CNS (24, 73), with the latter being transmitted via the
330 vagal nerve (74). Another study showed that vagotomy in mice prevents propagation of pathology
331 into the CNS (74), a finding that is parallel to a peripheral rotenone-related αSyn rat model in which
332 vagotomy reduced propagation of αSyn pathology (75), and to a human study that reported that
333 vagotomy in a Danish population also decreases the risk of PD (27). Similarly, after injection of PD
334 brain lysate and recombinant αSyn into the intestinal wall αSyn pathology trafficked through the
335 vagal nerve to the dorsal motor nucleus of the vagus (23). Others have shown that virus-based
336 expression of human αSyn in the medulla oblongata resulted in a transfer of αSyn towards rostral
337 brain regions in a rat model (76). The findings in these previous studies, along with the present
338 findings recall the Braak hypothesis and highlight the critical connection of the vagal nerve. Indeed, in
339 the present study, αSyn pathology was much more prominent in the reticular nucleus (including the

340 vagal area) and midbrain areas (compared to the rostral areas) 18 months post DSS colitis, suggesting
341 the potential involvement of this nerve in the accumulation of αSyn in the CNS.

342 Here, we report that individuals with IBD exhibit αSyn accumulation in the colon concomitant with
343 infiltrating monocytes/macrophages positive for αSyn. Employing a experimental model of IBD, we
344 provide proof-of-principle demonstrating that αSyn accumulated in the colon of (Thy1)-h[A30P]αSyn
345 transgenic and wildtype mice upon DSS colitis and that this process can be modulated by
346 monocyte/macrophage-related signaling. We further demonstrate that chronic DSS colitis in young
347 (Thy1)-h[A30P]αSyn transgenic mice robustly exacerbated αSyn accumulation in the aged brain
348 which was accompanied by reduced numbers of TH- and Nissl positive neurons in the nigra. The
349 present findings are in consonance with retrospective and cohort studies demonstrating a link between
350 IBD and PD in various populations including those in Taiwan, Denmark and the US (36, 37, 77),
351 although this may not be the case in all populations (78). The exact mechanisms connecting the gut
352 pathology to the pathology in the brain including the role of monocytes/macrophages, remain to be
353 established. In summary, this novel mouse model of a potential preclinical stage of PD recapitulated
354 the accumulation of αSyn in the ENS and the subsequent age-related development of brain pathology.
355 Together, our data suggest a critical role for intestinal inflammation in the initiation and progression
356 of PD.

357 **Methods**

358 ***Mice***

359 Male C57BL/6 wild type mice (Jackson Laboratories, Bar Harbor, USA), hemizygous Tg(Thy1-
360 SNCA*A30P)18Pjk ((Thy1)-h[A30P]αSyn) (39) and Tg(Thy1-SNCA*A30P)18Pjk crossed with
361 Cx3cr1tm1Litt ((Thy1)-h[A30P]αSyn /CX3CR1-def; homozygous for Cx3cr1-GFP knock-in allele;
362 (79) transgenic mice were used for the study. (Thy1)-h[A30P]αSyn transgenic mice express mutant
363 human αSyn under the neuron selective Thy1 promoter. (Thy1)-h[A30P]αSyn transgenic mice were
364 crossed to Cx3cr1-def transgenic mice which express eGFP replacing fractalkine gene expression. All
365 mice were maintained on a C57BL/6 background for more than 10 generations and under specific
366 pathogen-free conditions. To the extent possible, littermates were used in the experiments. Health
367 status was monitored daily during experiments.

368

369 ***Human Subjects***

370 Samples from patients with Crohn's disease (CD), ulcerative colitis (UC) or neither were provided by
371 the tissue bank, Institute of Pathology, University of Bern. Briefly, specimens were obtained from
372 patients who underwent surgical procedures at the University Hospital (Inselspital) in Bern,
373 Switzerland between 2004 and 2011. Three selected male patients previously clinically diagnosed
374 with UC with a reported disease duration > 6 year (n=3) and undergoing steroid therapy combined
375 with either metronidazole or mesalazine. CD patients were of mixed gender and aged 22-56 years
376 ranging from 2 months to 11 years post disease diagnosis undergoing treatment with either infliximab
377 or mesalazine in combination with steroids. Healthy subjects were of mixed gender with no report of
378 inflammatory bowel disease, aged 40-59. All samples contained the mucosa and submucosa regions
379 including minor parts of the circular muscle layer. Following surgical removal, tissue samples were
380 immediately immersed in O.C.T. compound (VWR International GmbH, Dietikon, Switzerland),
381 frozen in liquid nitrogen and stored at -80°C. Diagnosis of disease status was made according to
382 established criteria for histopathological analysis.

383

384 ***Experimental IBD in mice with DSS and LPS***

385 Paradigms for the induction of inflammation were either 1 week (acute) or 3-4 weeks (chronic) with
386 or without an incubation phase of 2, 6 or 18 months post application (**Figure 2**). Acute systemic
387 inflammation was induced by intraperitoneal Lipopolysaccharide (LPS) application (80) of 0.5 mg/kg
388 in 100 µl injection volume on day 1 and 4 (Sigma-Aldrich Chemie GmbH, Steinheim, Germany, LPS
389 055:B5). Acute colitis was induced by application of 36-50kDa Dextran Sodium Sulfate (DSS) (81)
390 (160110, MP Biomedicals, LLC, Illkirch, France) at 0%, 1%, 2.5% or 5% in autoclaved drinking
391 water for 5 continuous days respectively, followed by 2 days of water (1 DSS application cycle).
392 Chronic colitis was achieved by 4 repeating DSS application cycles. The DSS concentration during 4
393 weeks of chronic colitis was either 1% or 2.5% for 4 weeks or 2.5%-4% raised 0.5% every week for 4
394 weeks. Mice from same littermate group were randomized per cage into vehicle and inflammation
395 inducing agent.

396

397 ***IL-10 treatment and exposure measurement***

398 Two different forms of mouse IgG bound murine IL-10 (mIgG(v1)-mIL10 and mIgG(v2)-mIL10)
399 were diluted in pre-prepared sterile formulation buffer comprised of 0.5% mouse serum supplemented
400 with 25mM citrate, 300mM arginine to a final concentration of 0.75mg/ml and the pH adjusted to 6.7
401 on the day of application. Each mouse was treated once with 150 µg i.p concurrently with the
402 initiation of the acute colitis paradigm with 5% DSS. The concentrations of mIgG-mIL10 fusion
403 proteins in murine serum samples were determined by enzyme-linked immunosorbent assays (ELISA)
404 specific for the Fab moiety of the administered mIgG-mIL10 fusion protein. Biotinylated mIgG-
405 mIL10-specific target molecules were used for capturing, goat anti-mIg IgG-HRP conjugate and
406 peroxidase substrate ABTS was used for quantitative detection of mIgG-mIL10 fusion proteins.

407

408 ***Immunohistochemistry***

409 Animals were injected with a lethal dose of pentobarbital 150 mg/kg. Upon full anesthesia, mice
410 received transcardial perfusion with room temperature phosphate buffered saline (PBS). For
411 biochemical and immunohistochemical analysis, one section of either the proximal colon was fresh

412 frozen and stored at -80°C or post-fixed in 4% paraformaldehyde (PFA) solution for 24 h. Following
413 post-fixation, organs were incubated in 30% sucrose/PBS at 4°C for at least 48 h before further
414 processing. Subsequently, enteric tissue was cryotome-sectioned to 35 µm thick longitudinal sections
415 (approx. 1 cm length). The brain was collected and post-fixed for 24h in 4% PFA followed by 30%
416 sucrose in phosphate buffer until cryo-sectioning of floating sections at 40 µm. Histological analysis
417 of the colon was performed using standard hematoxylin staining. Immunohistochemical staining was
418 accomplished using the Vectastain Elite ABC Kits and Peroxidase Substrate Kit SK-4100 (Vector
419 Laboratories, Burlingame, CA, USA) or fluorescently labelled secondary antibodies (Alexa coupled
420 to dye 488, 555 or 647, Life Technologies, Zug, Switzerland). The following primary antibodies have
421 been used for overnight incubation at a dilution of 1:1000: monoclonal antibody to human α-synuclein
422 (sc-12767, Santa Cruz Biotechnology, Heidelberg, Germany), polyclonal antibody to murine α-
423 synuclein (Syn1, BD Transduction Laboratories, Allschwil, Switzerland), polyclonal antibody to the
424 peripheral neuronal marker Peripherin (Millipore Corporation, Billerica, MA, USA), and polyclonal
425 antibody to macrophage marker Iba1 (Wako Chemical GmbH, Neuss, Germany). To detect
426 phosphorylated αSyn (pSer129 pathology) in the free-floating brain sections, monoclonal antibody
427 (ab51253, Abcam, Cambridge, USA) to human αSyn was used at a dilution of 1:10000. Prior to the
428 pSer129 staining, the free-floating brain sections were incubated for 10 min at room temperature in a
429 phosphate buffered saline solution containing 10 µg/mL proteinase K (Cat # 25530015; Invitrogen,
430 California, USA). TH-immunoreactive cells were detected using a polyclonal antibody (657012,
431 Millipore Sigma) at a dilution of 1:1000. To measure the density of Nissl-positive cells, the TH-
432 stained cells were counter-stained with Cresyl violet. The slides were incubated in 0.1% Cresyl violet
433 solution for 9 min and then dehydrated in 95% and 100% ethanol and then xylene prior to
434 coverslipping with Cytoseal 60 mounting media (Thermo Fisher Scientific). Quantifications of the
435 blind-coded TH/Nissl stained slides were done using Stereoinvestigator (version 2017.01.1; MBF
436 Bioscience, Williams, VT, USA) on Imager M2 microscope (ZEISS) coupled to a computer. We
437 analyzed 5-7 nigral sections per animal, and a total of 7-8 animals per treatment group. We outlined
438 the substantia nigra pars compacta and counted every TH-immunoreactive and Nissl-positive cell in
439 that area and computed the number of cells per section, generating the mean cell density per animal.

440 We then calculated the mean density of cells per treatment group and analyzed the data using
441 unpaired Student's T-test after confirming normality and homoscedasticity in Prism 7.0 (GraphPad
442 Software).
443
444 ***Imaging and stereological quantification of αSyn deposits in enteric nervous system***
445 Imaging and stereological quantification was performed on a Zeiss Axio Imager Z2 fluorescence
446 microscope (Carl Zeiss AG, Jena, Germany). Leica TCS SP5 confocal system using an HCX PL APO
447 CS 40x 1.3 oil UV or an HCX PL APO LB 63x 1.4 oil UV objective was utilized for image recording.
448 Accumulation of αSyn in the ENS was assessed on a random set of 3 adjacent 35 µm thick, αSyn-
449 immunostained sections comprising the myenteric and submucosal neuronal plexuses. Analysis was
450 performed with the aid of Stereologer software (Stereo Investigator 10, MBF Bioscience, Williams,
451 VT, USA) as described previously (82). In the myenteric plexus ganglion volume was defined by
452 multiple outlined plexuses containing a range of 5-20 neuronal cells and quantified by the optical
453 fraction fractionator technique. In contrast to the myenteric plexus, the submucosa consists of
454 compact plexuses with 1-5 cells including interconnecting neurites. Therefore, the entire submucosa
455 was set as region of interest, analyzed with the area fraction fractionator technique. Results of the
456 submucosal plexus are displayed by percent area containing αSyn deposits. For the IL-10 experiment,
457 αSyn positive granules from immunofluorescence images were counted for each image. Granules
458 were filtered based on having a size between 12 and 50000 pixels and a minimal intensity value
459 greater than 300. The filtering step was included to exclude small background particles and
460 macrophages (very large spots). The counts were then aggregated to the animal level by summing the
461 granule counts of all images per animal and then normalizing for (i.e. dividing by) the number of
462 images for a given animal. Upon exploratory data analysis two animals were excluded: one mouse
463 because it only had one image and another due it being an outlier, based on its infiltration score and
464 image data.
465
466
467

468 ***Blinding***

469 For analyses of colon and brain tissue on slides, a second individual assigned unique codes to
470 stained slides. Therefore, the experimenter conducted the analyses blinded to the identity of the
471 mice. For randomization of treatment groups see above.

472

473 ***Quantification of leukocytes infiltration***

474 To determine the leukocyte covered area in the colon after LPS or DSS application, three adjacent
475 hematoxylin stained sections were quantified. Total area of colon sections and localizations of
476 leukocyte assemblies within the tissue architecture were identified and outlined utilizing Stereologer
477 Software (Stereo Investigator 6, MBF Bioscience, Williams, VT, USA). Percentage of leukocyte
478 covered area has been set in proportion to total area of the analyzed colon section. For the IL-10
479 experiment, hematoxilin stained colon slices were examined by an expert pathologist blinded to
480 treatment conditions. A score of 0-3 was assigned to each section for each of the 3 layers lamina
481 propria, submucosa and muscularis based on the degree of inflammatory infiltration. A score of 0
482 denoted no inflammation and a score of 3 indicated extensive infiltration. The mean of the values for
483 all 3 layers was taken as the final measure of leukocyte infiltration per mouse.

484

485 ***Quantification of αSyn/Iba1 double positive macrophages***

486 The number of α-syn+/Iba1+ positive cells was evaluated by quantification of 10 random regions in 2
487 adjacent sections of the proximal colon. The region of interest was set to contain the myenteric
488 plexus/circular muscle layer and the submucosal plexus. Cells were assessed for positive αSyn
489 staining and concomitant co-localization with the macrophage marker Iba1 was quantified.

490

491 ***Scoring of pSer129 pathology and brain heatmap***

492 We evaluated pSer129 pathology on a full series of immunostained coronal sections from 10 mice per
493 treatment group (i.e. water vs. DSS-treated groups) on blind-coded slides using a previously described
494 method (83). We visualized pathology from one hemisphere of all brain sections (apart from the

495 olfactory area) using NIKON Eclipse Ni-U microscope and assigned scores ranging from 0 to 4 to
496 each brain area based on the relative abundance of PK-resistant pSer129-positive inclusions (i.e. cell
497 bodies and neurites). In this case, 0 = no aggregates, 1 = sparse, 2 = mild, 3= dense, 4 = very dense.
498 For the heatmap, we obtained the average score values of each brain area for each treatment group.
499 The average data for each treatment group (n=10/ group) was then represented as a heatmap in a
500 sagittal mouse brain background (http://atlas.brain-
501 map.org/atlas?atlas=2#atlas=2&structure=771&resolution=16.75&x=
502 7755.7470703125&y=3899.625&zoom=-3&plate=100883867&z=5).
503
504 ***Densitometry of pSer129 αSyn brain pathology***
505 The density of pSer129 pathology in 12 major brain areas (reticular nucleus, pontine reticular nucleus,
506 periaqueductal gray, gray and white layer, reticular formation, substantia nigra, ventral tegmental
507 area, thalamus, hypothalamus, central amygdala, pallidum and striatum) were determined in the water
508 and DSS-treated animals. NIKON Eclipse Ni-U microscope was used to acquire 20x magnification
509 images (without condenser lens) from all the indicated brain areas, using the same exposure time for
510 all images. In all cases, images were acquired on three sections separated by 420 µm intervals
511 (localized between Bregma). We then processed the acquired images using Image J64 (84), created a
512 mask (to exclude background) that redirects to the original image for analysis, measured the total area
513 and the mean grey value of the area that had inclusions. For brain areas such as periaqueductal gray
514 that do not fill the entirety of the field to be analyzed, we drew a contour of the area and the analysis
515 was performed only within that contoured area. We subsequently calculated the grey value of the area
516 per square pixels for each image (i.e. A.U./px^2 = mean grey value x area stained/total area assessed).
517 Based on this, we calculated the average grey value per square pixels for each brain area for each
518 animal (n = 6 mice/group), and then extended this calculation to determine the average grey value per
519 square pixels for each treatment group and each of the twelve brain areas of interest.
520
521
522

523 ***mRNA expression***

524 To assess mRNA expression levels from the proximal colon, RNA was extracted from fresh frozen
525 tissue with MagnaLyser green beads (Roche Diagnostics, Mannheim, Germany) and Qiazol Lysis
526 (Reagent cat.no.79306, Hilden, Germany) purified on MagnaPure LC (HP Kit no.03542394001, F.
527 Hoffmann - La Roche AG, Rotkreuz, Switzerland) and amplified via real-time PCR (4ng
528 RNA/reaction; Lightcycler 480, Roche Diagnostics Corporation, Indianapolis, USA). Amplification
529 of mRNA was performed by using TaqMan probes for human or murine specific α-synuclein and for
530 selected cytokines/chemokines (Applied Biosystems Europe B.V., Zug, Switzerland). Target mRNA
531 was normalized to tissue-specific murine GAPDH levels and displayed as relative expression after 30
532 amplification cycles.

533

534 ***Statistics***

535 Statistical analysis of gut pathology and inflammation was performed using GraphPad Prism 6.04 or
536 7.0 software (GraphPad Software, Inc. La Jolla, CA, USA). The results are expressed as mean values
537 ± standard errors of the mean (SEM). Student's T-test (or Welch's T-test for unequal variances) was
538 used to compare two groups and ANOVA was used for multi-comparison of groups followed by
539 Tukey HSD post-hoc analysis. For the statistical analysis of the pSer129 αSyn brain pathology,
540 negative-binomial mixed-effects models with a random intercept for each sample were used to
541 analyze the dataset via the 'lme4' (http://lme4.r-forge.r-project.org/) package in R v 3.4.4. To analyze
542 the pSer129 αSyn cell count dataset, an offset for the total area examined was included to model the
543 densities. Linear contrasts with false discovery rate (FDR) adjustments were then used to test our
544 hypotheses and account for multiple testing (for brain area and experimental group). Like the pSer129
545 dataset, the Iba-1/αSyn-double positive dataset were analyzed using negative-binomial regression and
546 Tukey HSD adjusted contrasts to test our hypotheses.

547

548 For the mRNA expression analysis, data quality was assessed by inspecting the distribution of Cp
549 values of reference endogenous genes across samples, by inspecting the level of Cp variation between
550 technical replicates and by exploring the samples multivariate signal distribution as in a principal

551 component analysis. Relative gene expression levels were expressed as $2^{-(Cpgene - CpRef)}$. Statistical
552 analyses to assess the effect of the experimental conditions on the log2 gene expression levels were
553 done with linear models using the *limma* package (Bioconductor/R, Smyth, 2005). These analyses
554 were implemented in R v3.1.1.
555
556 For the statistical modelling of the effects of the IL-10 treatment on αSyn counts, as well as
557 infiltration scores, the levels for IgG1(v1)-IL10 and IgG1(v2)-IL10 treatment were compared to the
558 positive (vehicle/DSS) control. Additionally, since levels of the control antibody treatment (IgG1(v1))
559 were very similar to the positive control, the two groups were pooled in further contrasts in which
560 effects of individual antibodies or control IgG was assessed. For αSyn counts, a linear model on the
561 treatment groups with one-degree freedom contrasts was applied. For the infiltration score a Kruskal-
562 Wallis test, with the same contrasts was used.
563
564 ***Study approval***
565 The human subjects' study was conducted with the approval of the local Ethical Committee in Bern
566 No. 47/04. Written informed consent was obtained from each patient. The animal experiments were
567 approved by a Roche internal review board and the local authorities.

568 **Author contributions**

569 S.G., N.M. and L.S. planned and performed the in vivo experiments, colon immunostaining, analysis,
570 and quantification; S.G. and N.M. drafted a first version of the manuscript; E.Q. performed, imaged,
571 quantitated pSer129, TH and Nissl staining in the brain sections, and drafted a more advanced version
572 of the manuscript with J.A.S., who also provided helpful discussion. F.B. and K.O.S. supported the
573 image acquisition and image analysis for the colon samples; M.St. performed imaging and data
574 analysis of experiments with wildtype mice; G.D.P. and J.S.P. performed statistical analysis of the
575 DSS experiments; H.R. and M.H. performed mRNA analyses; M.Se. trained S.G. and L.S. on mouse
576 necropsy and supported their work; P.M. performed expert pathology staging on leukocyte
577 infiltration; T.E. and A.W. provided mIgG-mIL-10 fusion proteins and measured serum exposure;
578 Z.M. performed statistical analysis for the pSer129 αSyn immunohistochemistry data. M.L.E.G.
579 provided helpful discussion and project planning. A.H. co-mentored S.G. and N.M., performed expert
580 pathology staging on leukocyte infiltration and contributed to experimental planning. C.M. trained
581 S.G. on the colitis model, provided human tissue and expert input on the experimental IBD model.
582 M.B. and P.B. co-mentored Roche Postdoc Fellows S.G. and N.M., conceived and oversaw the study,
583 and performed experimental planning; M.B., P.B. and E.Q. wrote the final version of the manuscript.
584

585 **Acknowledgments**

586 We acknowledge the human donors for providing tissue used in this study. We thank Drs. L. Ozmen,
587 A. Bergadano, and A. Su for their tremendous support in maintaining the mouse colony and
588 establishing of relevant animal experiment licenses, and we are grateful to the animal care takers,
589 veterinarians and many unnamed staff at Roche for their valuable work with the mice in this study. In
590 addition, at Roche we thank Dr. K.G. Lassen for critical input to the paper, Dr. C. Ullmer for co-
591 mentoring S.G. and providing scientific input, Dr. L. Collin for helping with confocal imaging and we
592 are grateful to Dr. T. Kremer, N. Haenggi, D. Mona, A. Girardeau, and J. Messer for providing
593 support in tissue dissections and G. Walker and R. Lauria for technical support. Ms. E. Schulz from
594 VARI assisted with immunostaining of the brain tissue. We thank the Contract Research Organization
595 Frimorfo for carefully sectioning the brains for this study. We acknowledge Drs. L. Gaudimier (née

596 Chicha) and F. Pan-Montojo for scientific discussions early in the project and Dr. W. Zago from
597 Prothena for valuable scientific input. P.B. reports relevant grants from NIH (R01DC016519-01 and
598 5R21NS093993-02), Department of Defense (W81XWH-17-1-0534), The Michael J. Fox Foundation
599 for Parkinson's Research, and Cure Parkinson's Trust. Finally, we thank the Roche Postdoctoral
600 Fellowship Program for supporting S.G. and N.M.
601

602 **Conflicts of Interest**

603 At the time of the study S.G. and N.M. were Roche Postdoctoral Fellows employed by Roche and
604 L.S., F.B., G.D.P., J.S.P., K.O.S., H.R., M.H., M.Se. M.St., P.M., A.W., T.E., A.H. and M.B. are or
605 were fulltime employees or trainees at Roche and they may additionally hold Roche stock/stock
606 options. S.G. and L.S. are currently employees of Neurimmune AG, Schlieren, Switzerland. P.B. has
607 received commercial support as a consultant from Renovo Neural, Roche, Teva, Lundbeck A/S,
608 AbbVie, NeuroDerm, Fujifilm Cellular Dynamics, Living Cell Technologies, IOS Press Partners, and
609 Axial Biotherapeutics. Additionally, P.B. has received commercial support as a consultant from
610 Renovo Neural, Roche, Teva, Lundbeck A/S, AbbVie, NeuroDerm, Fujifilm Cellular Dynamics,
611 Living Cell Technologies, IOS Press Partners, Axial Biotherapeutics and CuraSen. Additionally, P.B.
612 has received commercial support for grants/research from Renovo, Roche, Teva, and Lundbeck. P.B.
613 has ownership interests in AcouSort AB. The other authors do not have conflicts of interest with
614 regard to this research.

References

1. Tysnes O-B, Storstein A. Epidemiology of Parkinson's disease. *J Neural Transm (Vienna)* 2017;124(8):901–905.

2. Spillantini MG et al. Alpha-synuclein in Lewy bodies. *Nature* 1997;388(6645):839–840.

3. Spillantini MG, Goedert M. Neurodegeneration and the ordered assembly of α-synuclein. *Cell Tissue Res.* 2017;373(1):137–148.

4. Braak H et al. Staging of the intracerebral inclusion body pathology associated with idiopathic Parkinson's disease (preclinical and clinical stages). *J. Neurol.* 2002;249 Suppl 3:III/1-5.

5. Del Tredici K, Braak H. Lewy pathology and neurodegeneration in premotor Parkinson's disease. *Mov. Disord.* 2012;27(5):597–607.

6. Polymeropoulos MH et al. Mutation in the alpha-synuclein gene identified in families with Parkinson's disease. *Science* 1997;276(5321):2045–2047.

7. Schrag A, Horsfall L, Walters K, Noyce A, Petersen I. Prediagnostic presentations of Parkinson's disease in primary care: a case-control study. *Lancet Neurol* 2015;14(1):57–64.

8. Gaenslen A, Swid I, Liepelt-Scarfone I, Godau J, Berg D. The patients' perception of prodromal symptoms before the initial diagnosis of Parkinson's disease. *Mov. Disord.* 2011;26(4):653–658.

9. Pont-Sunyer C et al. The onset of nonmotor symptoms in Parkinson's disease (the ONSET PD study). *Mov. Disord.* 2015;30(2):229–237.

10. Berg D et al. The PRIPS study: screening battery for subjects at risk for Parkinson's disease. *Eur. J. Neurol.* 2013;20(1):102–108.

11. Postuma RB, Gagnon J-F, Bertrand J-A, Génier Marchand D, Montplaisir JY. Parkinson risk in idiopathic REM sleep behavior disorder: preparing for neuroprotective trials. *Neurology* 2015;84(11):1104–1113.

12. Abbott RD et al. Frequency of bowel movements and the future risk of Parkinson's disease. *Neurology* 2001;57(3):456–462.

13. Savica R et al. Medical records documentation of constipation preceding Parkinson disease: A case-control study. *Neurology* 2009;73(21):1752–1758.

14. Mahlknecht P, Seppi K, Poewe W. The Concept of Prodromal Parkinson's Disease. *J Parkinsons Dis* 5(4):681–697.

15. Houser MC, Tansey MG. The gut-brain axis: is intestinal inflammation a silent driver of Parkinson's disease pathogenesis?. *npj Parkinson's Disease* 2017;3(1):3.

16. Braak H, Del Tredici K. Neuroanatomy and pathology of sporadic Parkinson's disease. *Adv Anat Embryol Cell Biol* 2009;201:1–119.

17. Braak H, de Vos RAI, Bohl J, Del Tredici K. Gastric alpha-synuclein immunoreactive inclusions in Meissner's and Auerbach's plexuses in cases staged for Parkinson's disease-related brain pathology. *Neurosci. Lett.* 2006;396(1):67–72.

18. Killinger BA et al. The vermiform appendix impacts the risk of developing Parkinson's disease. *Sci Transl Med* 2018;10(465):eaar5280.

19. Lee JM et al. The Search for a Peripheral Biopsy Indicator of α-Synuclein Pathology for Parkinson Disease. *J. Neuropathol. Exp. Neurol.* 2017;76(1):2–15.

20. Corbillé A-G et al. Evaluation of alpha-synuclein immunohistochemical methods for the detection of Lewy-type synucleinopathy in gastrointestinal biopsies. *Acta Neuropathol Commun* 2016;4:35.

21. Donadio V et al. A new potential biomarker for dementia with Lewy bodies: Skin nerve α-synuclein deposits. *Neurology* 2017;89(4):318–326.

22. Phillips RJ, Walter GC, Wilder SL, Baronowsky EA, Powley TL. Alpha-synuclein-immunopositive myenteric neurons and vagal preganglionic terminals: autonomic pathway implicated in Parkinson's disease?. *Neuroscience* 2008;153(3):733–750.

23. Holmqvist S et al. Direct evidence of Parkinson pathology spread from the gastrointestinal tract to the brain in rats. *Acta Neuropathol* 2014;128(6):805–820.

24. Breid S et al. Neuroinvasion of α-Synuclein Prionoids after Intraperitoneal and Intraglossal Inoculation. *J. Virol.* 2016;90(20):9182–9193.

25. Sargent D et al. "Prion-like" propagation of the synucleinopathy of M83 transgenic mice depends on the mouse genotype and type of inoculum. *J. Neurochem.* 2017;143(1):126–135.

26. Manfredsson FP et al. Induction of alpha-synuclein pathology in the enteric nervous system of the rat and non-human primate results in gastrointestinal dysmotility and transient CNS pathology. *Neurobiol. Dis.* 2018;112:106–118.

27. Svensson E et al. Vagotomy and subsequent risk of Parkinson's disease. *Ann Neurol.* 2015;78(4):522–529.

28. Stolzenberg E et al. A Role for Neuronal Alpha-Synuclein in Gastrointestinal Immunity. *JIN* 2017;9(5):456–463.

29. Devos D et al. Colonic inflammation in Parkinson's disease. *Neurobiol. Dis.* 2013;50:42–48.

30. Mogi M et al. Interleukin-1 beta, interleukin-6, epidermal growth factor and transforming growth factor-alpha are elevated in the brain from parkinsonian patients. *Neurosci. Lett.* 1994;180(2):147–150.

31. Brás J, Guerreiro R, Hardy J. SnapShot: Genetics of Parkinson's disease. *Cell* 2015;160(3):570-570.e1.

32. Witoelar A et al. Genome-wide Pleiotropy Between Parkinson Disease and Autoimmune Diseases. *JAMA Neurol* 2017;74(7):780–792.

33. Umeno J et al. Meta-analysis of published studies identified eight additional common susceptibility loci for Crohn's disease and ulcerative colitis. *Inflamm. Bowel Dis.* 2011;17(12):2407–2415.

34. Gardet A et al. LRRK2 is involved in the IFN-gamma response and host response to pathogens. *J. Immunol.* 2010;185(9):5577–5585.

35. Hakimi M et al. Parkinson's disease-linked LRRK2 is expressed in circulating and tissue immune cells and upregulated following recognition of microbial structures. *J Neural Transm (Vienna)* 2011;118(5):795–808.

36. Lin J-C, Lin C-S, Hsu C-W, Lin C-L, Kao C-H. Association Between Parkinson's Disease and Inflammatory Bowel Disease: a Nationwide Taiwanese Retrospective Cohort Study. *Inflamm. Bowel Dis.* 2016;22(5):1049–1055.

37. Peter I et al. Anti-Tumor Necrosis Factor Therapy and Incidence of Parkinson Disease Among Patients With Inflammatory Bowel Disease. *JAMA Neurol* 2018;75(8):939–946.

38. Wan Q-Y, Zhao R, Wu X-T. Older patients with IBD might have higher risk of Parkinson's disease. *Gut* 2018;gutjnl-2018-317103.

39. Kahle PJ et al. Subcellular localization of wild-type and Parkinson's disease-associated mutant alpha -synuclein in human and transgenic mouse brain. *J. Neurosci.* 2000;20(17):6365–6373.

40. Chassaing B, Aitken JD, Malleshappa M, Vijay-Kumar M. Dextran sulfate sodium (DSS)-induced colitis in mice. *Curr Protoc Immunol* 2014;104:Unit 15.25.

41. Weber B, Saurer L, Schenk M, Dickgreber N, Mueller C. CX3CR1 defines functionally distinct intestinal mononuclear phagocyte subsets which maintain their respective functions during homeostatic and inflammatory conditions. *Eur. J. Immunol.* 2011;41(3):773–779.

42. Medina-Contreras O et al. CX3CR1 regulates intestinal macrophage homeostasis, bacterial translocation, and colitogenic Th17 responses in mice. *J. Clin. Invest.* 2011;121(12):4787–4795.

43. Kostadinova FI et al. Crucial involvement of the CX3CR1-CX3CL1 axis in dextran sulfate sodium-mediated acute colitis in mice. *J. Leukoc. Biol.* 2010;88(1):133–143.

44. Kang S et al. Intestinal epithelial cell-derived semaphorin 7A negatively regulates development of colitis via αvβ1 integrin. *J. Immunol.* 2012;188(3):1108–1116.

45. Li B, Alli R, Vogel P, Geiger TL. IL-10 modulates DSS-induced colitis through a macrophage-ROS-NO axis. *Mucosal Immunol* 2014;7(4):869–878.

46. Braak H et al. Staging of brain pathology related to sporadic Parkinson's disease. *Neurobiol. Aging* 2003;24(2):197–211.

47. Neumann M et al. Misfolded proteinase K-resistant hyperphosphorylated alpha-synuclein in aged transgenic mice with locomotor deterioration and in human alpha-synucleinopathies. *J. Clin. Invest.* 2002;110(10):1429–1439.

48. Johnson ME, Stecher B, Labrie V, Brundin L, Brundin P. Triggers, Facilitators, and Aggravators: Redefining Parkinson's Disease Pathogenesis. *Trends Neurosci.* 2018;S0166-2236(18):30253–30254.

49. Shannon KM, Keshavarzian A, Dodiya HB, Jakate S, Kordower JH. Is alpha-synuclein in the colon a biomarker for premotor Parkinson's disease? Evidence from 3 cases. *Mov. Disord.* 2012;27(6):716–719.

50. Lebouvier T et al. Colonic biopsies to assess the neuropathology of Parkinson's disease and its relationship with symptoms. *PLoS ONE* 2010;5(9):e12728.

725 51. Kuo Y-M et al. Extensive enteric nervous system abnormalities in mice transgenic for artificial
726 chromosomes containing Parkinson disease-associated α-synuclein gene mutations precede central
727 nervous system changes. *Hum Mol Genet* 2010;19(9):1633–1650.

728 52. Luk KC et al. Pathological α-synuclein transmission initiates Parkinson-like neurodegeneration in
729 nontransgenic mice. *Science* 2012;338(6109):949–953.

730 53. Rey NL et al. Widespread transneuronal propagation of α-synucleinopathy triggered in olfactory
731 bulb mimics prodromal Parkinson's disease. *J Exp Med* 2016;213(9):1759–1778.

732 54. Al-Sadi RM, Ma TY. IL-1beta causes an increase in intestinal epithelial tight junction
733 permeability. *J. Immunol.* 2007;178(7):4641–4649.

734 55. Capaldo CT, Nusrat A. Cytokine regulation of tight junctions. *Biochim Biophys Acta*
735 2009;1788(4):864–871.

736 56. Forsyth CB et al. Increased Intestinal Permeability Correlates with Sigmoid Mucosa alpha-
737 Synuclein Staining and Endotoxin Exposure Markers in Early Parkinson's Disease. *PLOS ONE*
738 2011;6(12):e28032.

739 57. Gray MT, Munoz DG, Gray DA, Schlossmacher MG, Woulfe JM. Alpha-synuclein in the
740 appendiceal mucosa of neurologically intact subjects. *Mov. Disord.* 2014;29(8):991–998.

741 58. Labrie V, Brundin P. Alpha-Synuclein to the Rescue: Immune Cell Recruitment by Alpha-
742 Synuclein during Gastrointestinal Infection. *JIN* 2017;9(5):437–440.

743 59. Kelly LP et al. Progression of Intestinal Permeability Changes and Alpha-Synuclein Expression in
744 a Mouse Model of Parkinson's Disease. *Mov Disord* 2014;29(8):999–1009.

745 60. Haenseler W et al. Excess α-synuclein compromises phagocytosis in iPSC-derived macrophages.
746 *Sci Rep* 2017;7(1):9003.

61. Takagawa T et al. An increase in LRRK2 suppresses autophagy and enhances Dectin-1–induced immunity in a mouse model of colitis. *Science Translational Medicine* 2018;10(444):eaan8162.

62. Erickson MA, Hansen K, Banks WA. Inflammation-induced dysfunction of the low-density lipoprotein receptor-related protein-1 at the blood-brain barrier: protection by the antioxidant N-acetylcysteine. *Brain Behav. Immun.* 2012;26(7):1085–1094.

63. Cardoso FL et al. Exposure to Lipopolysaccharide and/or Unconjugated Bilirubin Impair the Integrity and Function of Brain Microvascular Endothelial Cells. *PLOS ONE* 2012;7(5):e35919.

64. Erny D et al. Host microbiota constantly control maturation and function of microglia in the CNS. *Nat. Neurosci.* 2015;18(7):965–977.

65. Sampson TR et al. Gut Microbiota Regulate Motor Deficits and Neuroinflammation in a Model of Parkinson's Disease. *Cell* 2016;167(6):1469-1480.e12.

66. Chen SG et al. Exposure to the Functional Bacterial Amyloid Protein Curli Enhances Alpha-Synuclein Aggregation in Aged Fischer 344 Rats and *Caenorhabditis elegans*. *Scientific Reports* 2016;6:34477.

67. Wendeln A-C et al. Innate immune memory in the brain shapes neurological disease hallmarks. *Nature* 2018;556(7701):332–338.

68. Steiner JA, Quansah E, Brundin P. The concept of alpha-synuclein as a prion-like protein: ten years after. *Cell Tissue Res.* 2018;373(1):161–173.

69. Recasens A et al. Lewy body extracts from Parkinson disease brains trigger α-synuclein pathology and neurodegeneration in mice and monkeys. *Ann. Neurol.* 2014;75(3):351–362.

70. Hansen C et al. α-Synuclein propagates from mouse brain to grafted dopaminergic neurons and seeds aggregation in cultured human cells. *J Clin Invest* 2011;121(2):715–725.

71. Angot E et al. Alpha-Synuclein Cell-to-Cell Transfer and Seeding in Grafted Dopaminergic Neurons In Vivo. *PLOS ONE* 2012;7(6):e39465.

72. Desplats P et al. Inclusion formation and neuronal cell death through neuron-to-neuron transmission of α-synuclein. *Proc Natl Acad Sci U S A* 2009;106(31):13010–13015.

73. Sacino AN et al. Intramuscular injection of α-synuclein induces CNS α-synuclein pathology and a rapid-onset motor phenotype in transgenic mice. *Proc Natl Acad Sci U S A* 2014;111(29):10732–10737.

74. Uemura N et al. Inoculation of α-synuclein preformed fibrils into the mouse gastrointestinal tract induces Lewy body-like aggregates in the brainstem via the vagus nerve. *Molecular Neurodegeneration* 2018;13:21.

75. Pan-Montojo F et al. Environmental toxins trigger PD-like progression via increased alpha-synuclein release from enteric neurons in mice. *Sci Rep* 2012;2:898.

76. Ulusoy A et al. Neuron-to-neuron α-synuclein propagation in vivo is independent of neuronal injury. *Acta Neuropathol Commun* 2015;3(13):1–13.

77. Villumsen M, Aznar S, Pakkenberg B, Jess T, Brudek T. Inflammatory bowel disease increases the risk of Parkinson's disease: a Danish nationwide cohort study 1977-2014. *Gut* 2018;68(1):18–24.

78. Fujioka S et al. Occurrence of Crohn's disease with Parkinson's disease. *Parkinsonism & Related Disorders* 2017;37:116–117.

79. Jung S et al. Analysis of fractalkine receptor CX(3)CR1 function by targeted deletion and green fluorescent protein reporter gene insertion. *Mol. Cell. Biol.* 2000;20(11):4106–4114.

80. Kitazawa M, Oddo S, Yamasaki TR, Green KN, LaFerla FM. Lipopolysaccharide-induced inflammation exacerbates tau pathology by a cyclin-dependent kinase 5-mediated pathway in a transgenic model of Alzheimer's disease. *J. Neurosci.* 2005;25(39):8843–8853.

81. Schenk M, Bouchon A, Seibold F, Mueller C. TREM-1--expressing intestinal macrophages crucially amplify chronic inflammation in experimental colitis and inflammatory bowel diseases. *J. Clin. Invest.* 2007;117(10):3097–3106.

82. Grathwohl SA et al. Formation and maintenance of Alzheimer's disease β-amyloid plaques in the absence of microglia. *Nat Neurosci* 2009;12(11):1361–1363.

83. Rey NL et al. Spread of aggregates after olfactory bulb injection of α-synuclein fibrils is associated with early neuronal loss and is reduced long term. *Acta Neuropathol* 2017;1–19.

84. Schneider CA, Rasband WS, Eliceiri KW. NIH Image to ImageJ: 25 years of image analysis. *Nat. Methods* 2012;9(7):671–675.

802 **Figures and figure legends**

Grathwohl et al., Figure 1

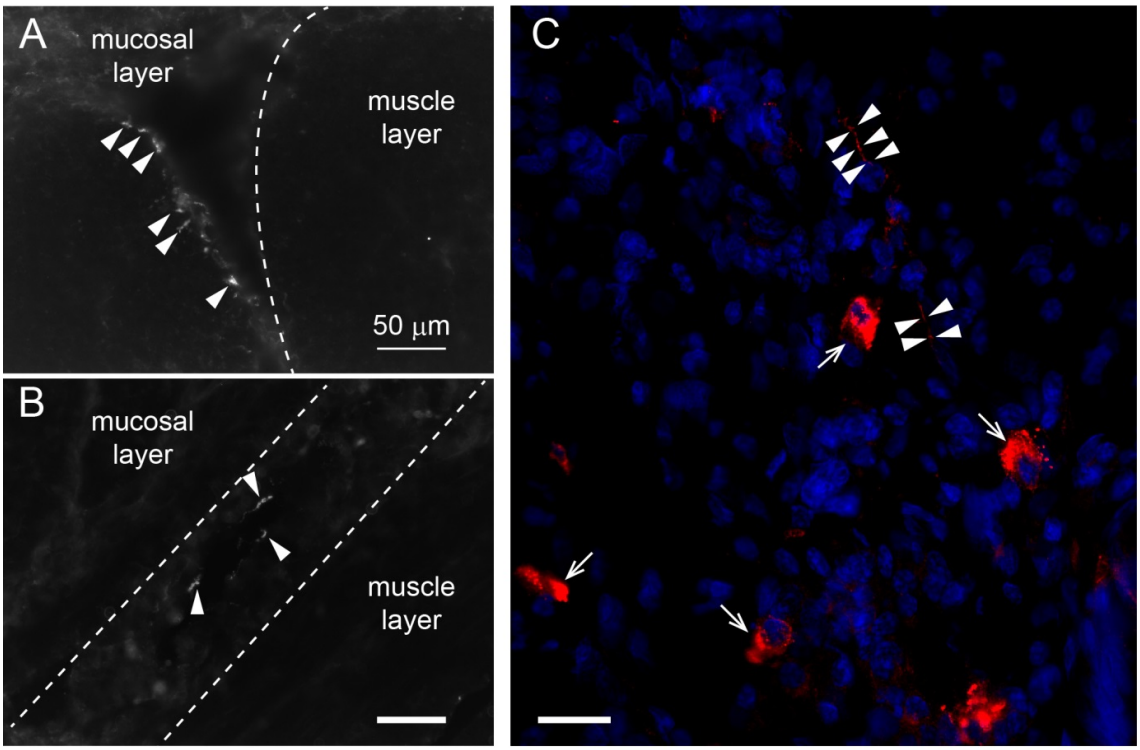

803

804 **Figure 1**

805 **Alpha-Synuclein inclusions in the enteric nervous system and in macrophages of patients with**
806 **inflammatory bowel disease. (A, B)** Immunofluorescence images of αSyn inclusions (Syn1) in the
807 submucosal region of 10 µm cryo-sections from colons of patients with colitis ulcerosa. Arrow heads
808 point to neuritic features indicating presence of inclusions in enteric nerves. Scale bar 50 µm. **(C)**
809 Close-up of a colonic region with active leukocyte infiltration in a patient with ulcerative colitis.
810 Immunoreactivity for αSyn (red) was observed in neuritic features (arrow heads) as well as in
811 individual leukocytes (arrows). Nuclei are shown in blue (DAPI). Scale bar 20 µm.

812

813

814

Grathwohl et al., Figure 2

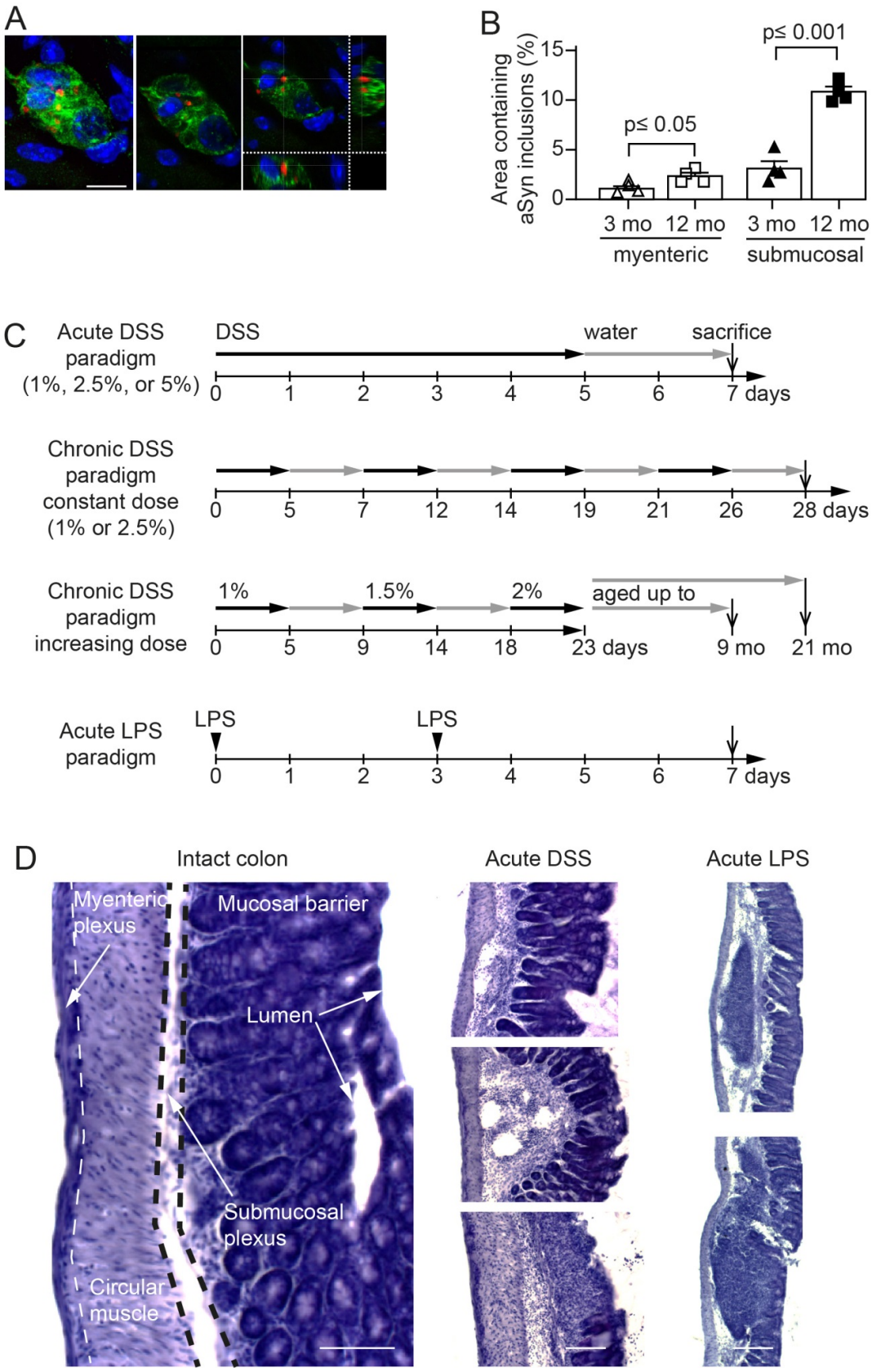

815

816 **Figure 2**

817 **Age dependent increase of intracellular αSyn accumulation in enteric nervous system of**
818 **heterozygous (Thy1)-h[A30P]αSyn transgenic mice and setup of the experimental colitis**
819 **paradigms. (A)** Confocal microscopy imaging of the granular inclusions of human αSyn (red,
820 antibody clone 211) within the ganglia of the submucosal plexus (green, peripherin; blue,
821 DAPI/nuclei) of heterozygous (Thy1)-h[A30P]αSyn transgenic mice. Scale bar, 100 µm. **(B)**
822 Stereological quantification of normally occurring human αSyn inclusions in the myenteric and
823 submucosal plexuses of 3 and 12 months old heterozygous (Thy1)-h[A30P]αSyn transgenic mice (n =
824 4 per group; mean and S.E.M. are shown; Student t-test between the two age groups in each region).
825 **(C)** Setup of experimental colitis paradigms employing dextran sodium sulfate (DSS, per os in
826 drinking water). Additionally, peripheral inflammation was induced by bacterial lipopolysaccharide
827 (LPS, intraperitoneal injection). For some DSS paradigms mice were sacrificed after an additional 2, 9
828 or 18-month of aging time on normal water **(D)** Hematoxylin staining of 35 µm thick colon sections
829 of 3 months old heterozygous (Thy1)-h[A30P]αSyn transgenic mice. Organizational layers of the
830 intact colon (left panel). Representative images of various severity degrees of DSS-driven colitis from
831 weak leukocyte infiltration (top panel of acute DSS) to mucosal ulceration (lowest panel of acute
832 DSS). Note the different appearance of enteric inflammation in acute LPS-driven peripheral
833 inflammation compared with DSS; e.g., confined immune cell clustering and lymphoid hyperplasia;
834 intact mucosal layer. Scale bar 50 µm (intact colon), 100 µm (acute DSS), and 200 µm (LPS).
835

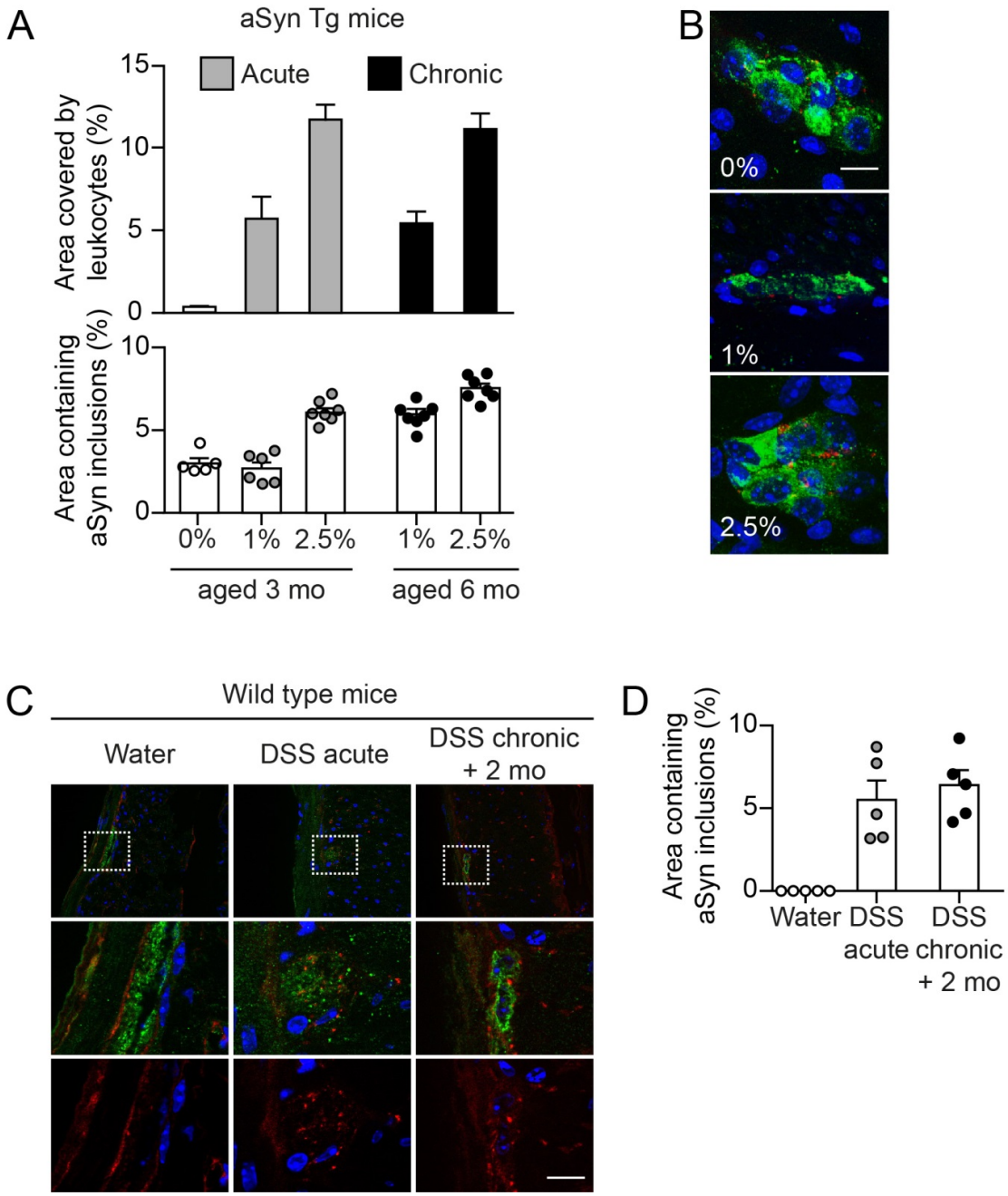

Figure 3

Colitis severity and duration-dependent aggravation of accumulation of αSyn inclusions in the colonic submucosal plexus of heterozygous (Thy1)-h[A30P]αSyn transgenic and wild type mice. **(A)** DSS dose-dependent increase of leukocyte infiltration in the acute and chronic paradigm. The highest acute dose (2.5%) and the two constant chronic doses led to an increase of αSyn inclusions in

842 the submucosal plexus (stereological quantification of αSyn inclusions in the submucosal plexus of 3
843 and 6 months old heterozygous (Thy1)-h[A30P]αSyn transgenic mice (n = 5-7 per group; mean and
844 s.e.m. are shown). **(B)** Representative 2D stacks of confocal images of increasing abundance of αSyn
845 inclusions (red, clone 211 antibody) in a ganglion of the submucosal plexus (green, peripherin) with
846 cellular nuclei in blue (DAPI). Scale bar 200 µm. **(C)** Overview of colonic region of 3-month-old
847 wildtype mice (top row) exposed to water or acute DSS (5%) with immunofluorescence analysis of
848 murine aSyn load in the colon performed immediately after colitis or exposed to constant chronic DSS
849 (2.5%) and analysis after aging on normal water for another 2 months. White dotted rectangles
850 indicate area that was zoomed out below illustrating in more detail the granular murine αSyn
851 inclusions (red, syn1 antibody) after DSS colitis in the submucosal plexus (green, peripherin
852 antibody). The lower panel shows DAPI and αSyn inclusions without the peripherin channel. Scale
853 bar for the lower two panels 200 µm. **(D)** Stereological quantification of granular murine αSyn
854 inclusions in the submucosal plexus of wildtype mice right after acute DSS colitis or after 2 months of
855 recovery from a 4-week chronic DSS colitis (n = 5 per group). Note the immunoreactivity for the
856 physiological, non-granular αSyn in the enteric nerves of the water group. The significant increase in
857 the DSS groups is evident without a statistical test.
858

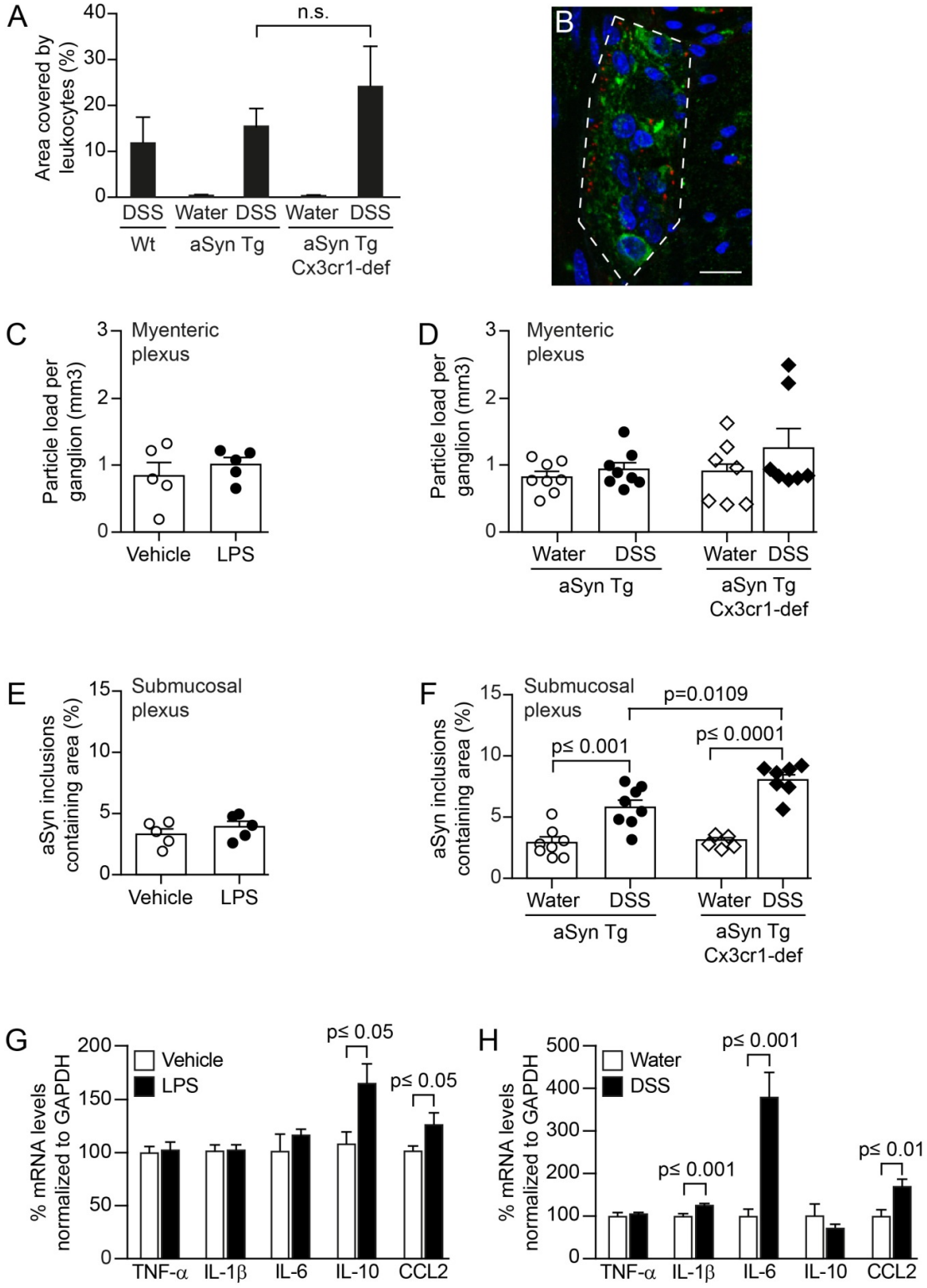
A
Area covered by leukocytes (%)
n.s.
DSS
Water
DSS
Water
DSS
Wt
aSyn Tg
aSyn Tg Cx3cr1-def
B
C
Myenteric plexus
Particle load per ganglion (mm3)
Vehicle
LPS
D
Myenteric plexus
Particle load per ganglion (mm3)
Water
DSS
Water
DSS
aSyn Tg
aSyn Tg Cx3cr1-def
E
Submucosal plexus
aSyn inclusions containing area (%)
Vehicle
LPS
F
Submucosal plexus
p=0.0109
p≤ 0.001
p≤ 0.0001
aSyn inclusions containing area (%)
Water
DSS
Water
DSS
aSyn Tg
aSyn Tg Cx3cr1-def
G
Vehicle
LPS
p≤ 0.05
p≤ 0.05
% mRNA levels normalized to GAPDH
TNF-α
IL-1β
IL-6
IL-10
CCL2
H
Water
DSS
p≤ 0.001
p≤ 0.001
p≤ 0.01
% mRNA levels normalized to GAPDH
TNF-α
IL-1β
IL-6
IL-10
CCL2

861 **Figure 4**

862 **Colitis induced by peroral DSS but not peritoneal LPS enhances αSyn accumulation in the**
863 **colonic submucosal plexus of heterozygous (Thy1)-h[A30P]αSyn transgenic mice and can be**
864 **aggravated by lack of Cx3cr1 signaling. (A)** Administration of DSS (acute 5%) induces leukocyte
865 infiltration in wildtype, (Thy1)-h[A30P]αSyn transgenic (αSyn Tg) and Cx3cr1- deficient (Thy1)-
866 h[A30P]αSyn transgenic mice (αSyn Tg Cx3cr1-def). Relevant increase compared to water group is
867 evident without a statistical test. **(B)** Representative 2D stacks of confocal images of intracellular
868 granular αSyn inclusions (red, clone 211 antibody) in a ganglion of the myenteric plexus (green,
869 peripherin) with cellular nuclei in blue (DAPI). Scale bar 50 µm. Due to the clear distinction of the
870 large ganglia in the myenteric plexus granular features of the αSyn inclusions could be stereologically
871 quantified as particle load per ganglion **(C, D)**, whereas the αSyn inclusions in the elongated and more
872 diffuse appearing ganglia of the submucosal plexus were stereologically quantified as % area **(E, F)**.
873 Note the slight but significant mean increase of αSyn inclusions in Cx3cr1- deficient (Thy1)-
874 h[A30P]αSyn transgenic mice compared to (Thy1)-h[A30P]αSyn transgenic mice (Two-way ANOVA
875 with Tukey post hoc test). Gene expression analysis of selected cytokines in the colon of (Thy1)-
876 h[A30P]αSyn transgenic mice that received either acutely LPS **(G)** or DSS **(H)** compared to their
877 respective vehicle or water controls. Note the strong increase in IL-6 and the lack of elevation of IL-
878 10 in the DSS paradigm compared to the LPS paradigm indicating a different inflammatory colonic
879 milieu despite the abundant leukocyte infiltration in both paradigms. n = 5-8 per group; mean and
880 s.e.m.; Student's t-test between inflammatory agent and vehicle for individual cytokines.
881

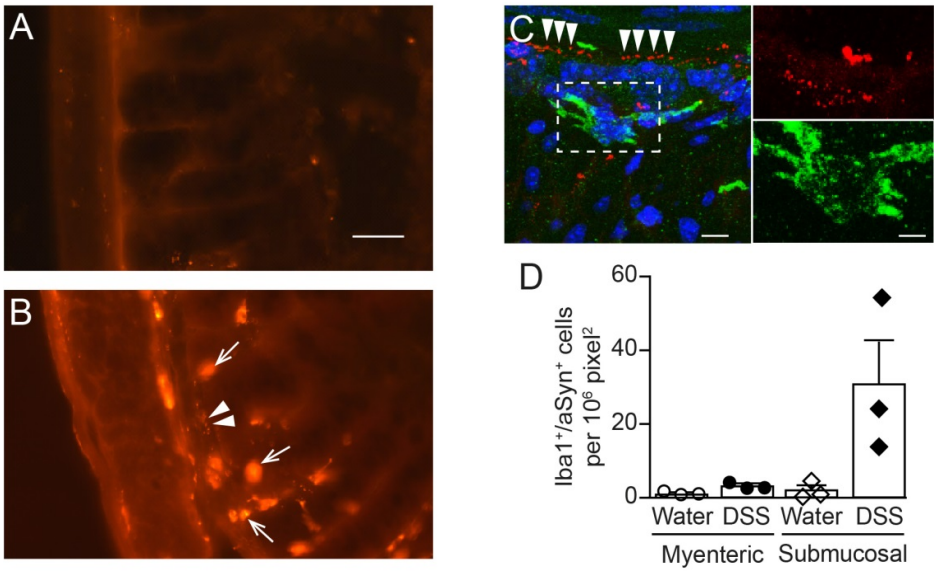

Figure 5

Alpha-synuclein co-localizes with ENS and macrophages upon DSS colitis in αSyn transgenic mice. (A, B) Immunofluorescence image of αSyn staining in colonic region of (Thy1)-h[A30P]αSyn transgenic mice on water **(A)** or after acute DSS colitis (2.5%) **(B)**. Note the small dotted structures of the typical αSyn inclusions in the submucosal plexus (arrow heads) and the large features of immunoreactivity which localize to apparent infiltrating leukocytes (arrows), similar to what was observed in IBD patients in Figure 1. Scale bar 100 µm. **(C)** 2D stacks and close-up of confocal images co-localizing αSyn (red) with the macrophage marker Iba-1 (green) in the colon of a (Thy1)-h[A30P]αSyn transgenic mouse after DSS colitis. Note the dotted structures of the typical αSyn inclusions in the submucosal plexus (arrow heads). Scale bar 40 µm and 13 µm for the close-up. **(D)** Quantification of numbers of Iba-1/αSyn-double positive macrophages (n = 3 per group; mean and S.E.M.; difference in submucosal plexus of DSS group vs water is obvious without a statistical test).

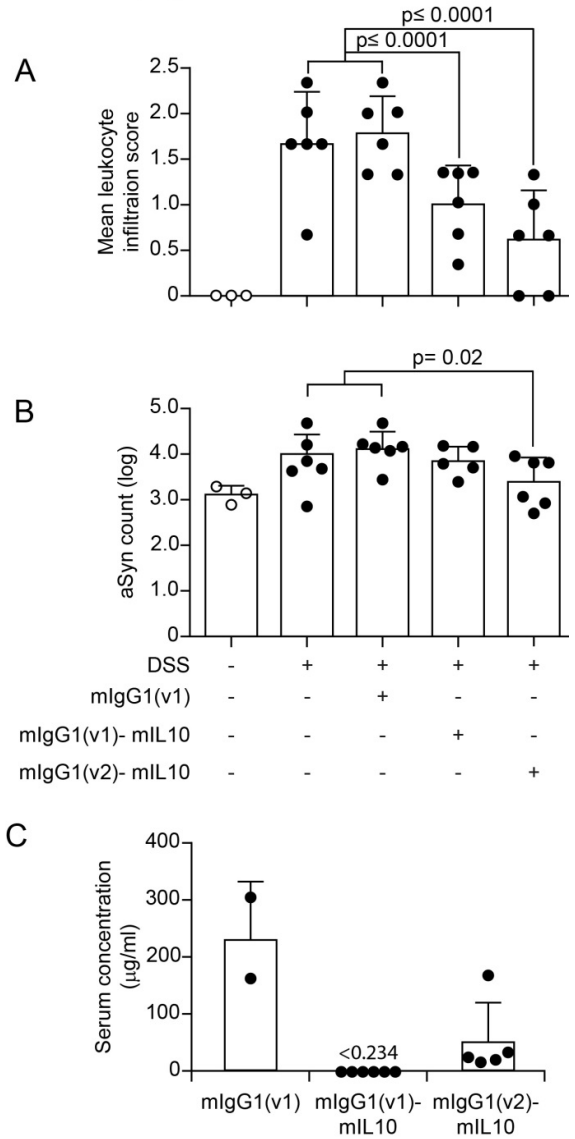

Figure 6

Systemic IL-10 ameliorates DSS colitis and associated local αSyn accumulation in (Thy1)-h[A30P]αSyn transgenic mice. Two different recombinantly engineered and murine IgG1-fused forms of murine IL-10 (mIgG1(v1)-mIL10 and mIgG1(v2)-mIL10) were administered i .p. in an acute DSS paradigm (5%) with (Thy1)-h[A30P]αSyn transgenic mice. Vehicle and the mIgG1(v1) alone served as untreated controls. **(A)** Leukocyte infiltration was assessed by visual scoring and **(B)** inclusion features of αSyn were stereologically and semi-automatically quantified and result log scaled for statistical analysis. Both the vehicle group and the mIgG1(v1) group had similar levels of

905 leukocyte infiltration and αSyn inclusions and were merged for the statistical analysis to compare with
906 the IL-10 treated groups. Both forms of IL-10 ameliorated leukocyte infiltration whereas mIgG1(v2)-
907 mIL10 also blocked the appearance of αSyn inclusions significantly (n = 3-6 per group; mean and
908 s.e.m.; one-way ANOVA and Tukey post hoc test). **(C)** Persistent exposure mIgG1(v2)-mIL10 versus
909 mIgG1(v1)-mIL10 (lower limit of detection is indicated) as measured in serum at the end of the in
910 vivo phase corresponds with beneficial treatment effects on αSyn readout observed above. The
911 mIgG1(v1) was only measured in two mice.
912
913
914
915
916
917
918
919

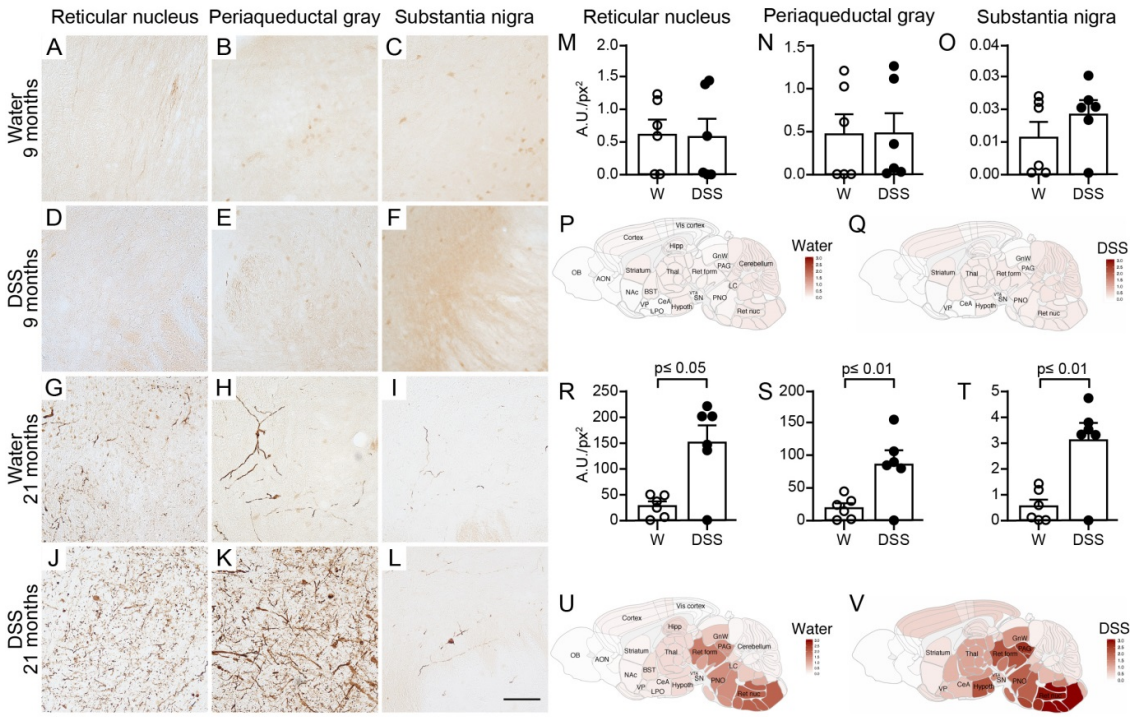

Figure 7

A single chronic DSS colitis insult causes an age-dependent accumulation of proteinase K resistant pSer129-αSyn in various brain regions of (Thy1)-h[A30P]αSyn transgenic mice. A 3-week chronic increasing dose DSS paradigm was performed with 3-month old (Thy1)-h[A30P]αSyn transgenic mice. After recovering and further aging, various brain regions were analyzed for proteinase K resistant pSer129-αSyn immunoreactivity in 9-month **(A-F)** and 21-month old **(G-L)** mice, respectively. Densitometric quantification of pSer129-αSyn immunoreactivity in different brain regions in 9-month **(M-O)** and 21-month old mice **(R-T)** (n=6 mice per group). Statistical analyses were performed using negative-binomial mixed-effects models adjusting for multiple comparisons. Representative heatmap of the average distribution scores of pSer129-αSyn immunoreactivity for each treatment group in varying brain regions in all the 9-month **(P-Q)** and 21-month old **(U-V)** mice was generated in a sagittal mouse brain (n=10 mice per group). Scale bars: 500 µm.

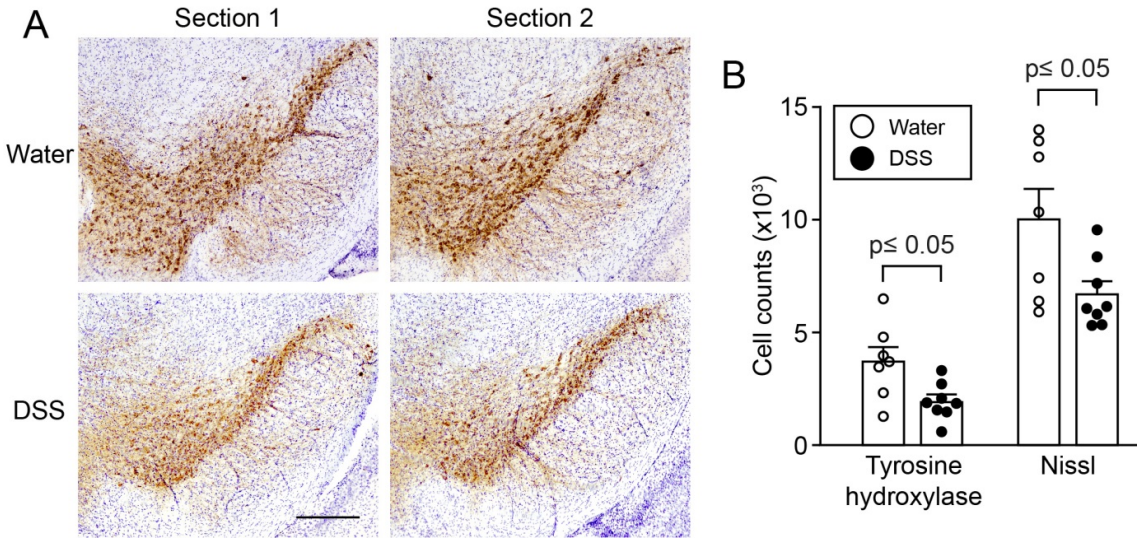

935

936 **Figure 8**

937 **Loss of tyrosine hydroxylase and Nissl positive cells in the substantia nigra of (Thy1)-**
938 **h[A30P]αSyn transgenic mice at 18 months post recovery from DSS colitis.** (Thy1)-h[A30P]αSyn
939 transgenic mice that were exposed to a chronic DSS-colitis paradigm at 3 months and were aged to 21
940 months showed a significant loss of mean count of cells with tyrosine hydroxylase (TH)
941 immunoreactivity and cellular Nissl staining in the substantia nigra compared to age-matched
942 littermate mice in the group that did not experience DSS colitis (water). **(A)** Representative images of
943 two levels of the substantia nigra in one mouse per group. **(B)** Stereological quantification of cells
944 positive for TH or Nissl (n=7-8 mice per group). Statistical analyses of the TH dataset was performed
945 using Student's T-test, while Welch's T-test was used for the Nissl dataset to adjust for unequal
946 variances. Scale bar: 500 µm.

947